Self-organized Anodic TiO_2 Nanotube Layers: Influence of the Ti substrate on Nanotube Growth and Dimensions

Hanna Sopha[a], Ales Jäger[b], Petr Knotek[c], Karel Tesař[b], Marketa Jarosova[d], Jan M. Macak[a,*,1]

[a]*Center of Materials and Nanotechnologies, Faculty of Chemical Technology, University of Pardubice, Nam. Cs. Legii 565, 53002 Pardubice, Czech Republic*
[b]*Laboratory of Nanostructures and Nanomaterials, Institute of Physics of the CAS, v.v.i., Na Slovance 2, 182 21 Prague 8, Czech Republic*
[c]*Department of General and Inorganic Chemistry, Faculty of Chemical Technology, University of Pardubice, Studentska 573, 532 10 Pardubice, Czech Republic*
[d]*Institute of Physics of the CAS, v.v.i., Cukrovarnicka 10, 162 00 Prague 6, Czech Republic*
**Corresponding Author: e-mail: jan.macak@upce.cz,* [1] ISE Member
Phone: +420-466 037 401

Abstract

In this contribution, various Ti thin substrates were explored and compared for the anodic growth of self-organized TiO_2 nanotube layers for the first time. In order to evaluate differences in the electrochemical anodization characteristics and the tube dimensions, five different Ti substrates from four established suppliers were anodized in the widely used ethylene glycol electrolytes containing 88 mM NH_4F and 1,5 vol.% water. Two anodizations were carried out to elucidate an influence of the pre-anodized substrates used for the second anodization. By thorough evaluation of the nanotube dimensions, large variations between the dimensions of the nanotubes were found for the different substrates, ranging from ~32 µm to ~50 µm for the nanotube length and from ~109 nm to ~127 nm for the nanotube diameter after the second anodization. Upon AFM measurements, Goodfellow Ti substrates (99.99 % purity), yielded the smoothest surface and the highest degree of ordering from all substrates. Moreover, considerably different consumption of Ti substrates via anodization was revealed by profilometric measurements between the original non-anodized part of the Ti substrates, and the anodized part after the removal of the nanotube layer. Orientation imaging

microscopy revealed considerable differences in the size and orientation of the substrate grains.

Keywords: Titanium; Anodization; Titanium dioxide; Nanotubes; Ordering

1. Introduction

Since their introduction [1,2], TiO_2 nanotube layers produced by anodization of Ti have attracted wide interest due to their application in various fields, such as dye-sensitized solar cells [3-7], sensors [8-10] or photocatalysis [11-13]. Overviews about applications are also given in several review articles [14-16]. During the past 10 years, considerable attention was given on the control of the nanotube dimensions, i.e. length and diameter, and the ordering of the nanotubes. The nanotube diameter and length can be controlled by the applied potential, the anodization time and the electrolyte used for anodization [17-19]. Thus, the first generation of TiO_2 nanotubes produced in HF-containing electrolytes did not exceed a length of approximately 500 - 600 nm due to a fast dissolution of TiO_2 by HF [20]. Later on, other electrolytes, i.e. glycerol [21, 22] and ethylene glycol [23] based electrolytes, containing NH_4F instead of HF were explored, which enabled researchers to produce a wide range of nanotube layers with different aspect ratios.

It is known from the sister material – porous alumina – that hexagonal packing and improved ordering of pores in general is crucial for numerous other applications, such as waveguides and photonic crystals [24, 25]. Therefore, efforts have been carried out to improve the degree of ordering of TiO_2 nanotube arrays. The simplest way to produce ordered TiO_2 nanotubes turned out to be the repetitive anodization of the same substrate, after the removal of the nanotube layer grown during the first anodization, and applying a second anodization step [26-29]. Other attempts included either polishing of the Ti surface by various means (such as

chemical, mechanical and/or electro- polishing) to reduce its roughness, [30, 31], or pre-texturing of Ti by a nanoimprinting process [32]. However, the degree of ordering and the ordering range are very likely strongly influenced by the microstructure of Ti, which has numerous grain boundaries. Nevertheless, to the best of our knowledge no studies have yet been reported that compare different Ti substrates in terms of roughness, microstructure and electrochemical characteristics, and their influence on the nanotube characteristics.

Therefore, in this work, five different Ti substrates from established suppliers were investigated (and compared) with respect to the electrochemical characteristics of the nanotube growth, and their resulting dimensions. Two repetitive anodizations on each substrate were performed followed by a thorough check of all resulting layers by scanning electron microscope (SEM) Furthermore, the roughness of the Ti substrates after the second anodization was analysed by atomic force microscope (AFM). Additionally, the average depth of the anodized area was measured using a profilometer. Finally, the microstructure of the substrates was investigated by electron backscatter diffraction (EBSD) technique.

2. Experimental

Five types of Ti substrates of different purities commonly used for the TiO_2 nanotube growth by researchers worldwide were purchased from four established suppliers for comparison; Sigma-Aldrich (0.127 mm, 99.7 % purity, marked as SiAl), Advent Materials (0.125 mm, 99.6+% purity, marked as AM), Chempur (0.125 mm, 99.6% purity, marked as CP), Goodfellow (0.125 mm, 99.6+% purity, marked as GoFe99.6+%) and Goodfellow (0.125 mm, 99.99% purity, marked as GoFe99.99%).

The Ti substrates were degreased prior to anodization by sonication in isopropanol and acetone, then rinsed with isopropanol and dried in air. The electrochemical setup consisted of a 2 electrode configuration using a platinum foil as the counter electrode, while the Ti

substrates (working electrodes) were pressed against an O-ring of the electrochemical cell, leaving 1 cm^2 open to an electrolyte. Electrochemical experiments were carried out at room temperature employing a high-voltage potentiostat (PGU-200V, IPS Elektroniklabor GmbH). For the electrolyte, ethylene glycol was used containing 1.5 vol.% deionized water and 88 mM NH_4F. All electrolytes were prepared from reagent grade chemicals. Before use, all electrolytes were aged for 9 hours by anodization of blank Ti substrates at 60 V under the same conditions as for the main anodization experiments. If not stated otherwise, Ti substrates were anodized for 14 hours during the first anodization and for 6 hours during the second anodization. The first nanotube layer was removed by cathodic reduction of the substrate, as reported previously [33], followed by sonication of Ti in isopropanol, in preparation for the second anodization. For all experiments new electrolytes were employed, which were freshly aged and not used in any previous anodizations, resulting in electrolytes of the same age for all anodizations. At the beginning of the anodization process, the potential was swept from 0 V to 60 V with a sweeping rate of 1 V/s. After anodization, the Ti substrates were rinsed and sonicated in isopropanol and dried.

The structure and morphology of the TiO_2 nanotubes were characterized by a field-emission SEM (JEOL JSM 7500F). Dimensions of the nanotubes were measured and statically evaluated using proprietary Nanomeasure software. For each condition used in this work, average values and standard deviations were calculated from at least 3 different locations on 2 samples of each condition, with a high number of measurements ($n \geq 100$).

An Atomic Force Microscope (AFM, Solver Pro M, NT-MDT) was used to evaluate the surface topography of the substrates in semi-contact mode following the second anodization, on the area of 5x5 μm^2, according to conditions mentioned elsewhere [34]. The roughness (root mean square - RMS) of the surface of Ti substrates was monitored by a digital holographic microscope (DHM, DHMR1000, Lyncée Tec) from a representative area

415x415 μm^2 [35]. The depth profiles of the craters left on the substrates after removing the nanotube layers after the second anodization were measured using a mechanical profilometer (SSC-01, RMI Ltd.) on the length scale 500 μm with the step of 0.5 μm [36]. The raw data from the profilometer was corrected for the long-distance deflection of the material´s surface by the 2^{nd} order polynomial function.

The chemical composition of the substrates was determined by glow-discharge optical emission spectroscopy (GD-OES, Spectruma GDA 750 HR). A direct current method with a voltage of 1200 V, a current 15 mA and a chamber pressure of ~3.5 hPa was utilized for the measurements. Certified reference materials were used for the measurement calibration. The data represent an integral value of the chemical composition through a depth profile in the interval from ~50 μm to ~70 μm below the surface of the substrates.

Microstructural information about polycrystalline Ti substrates was acquired by EBSD technique using a Microprobe JEOL 733 or Dual Beam FEI Quanta 3D FEG; both fitted with an EDAX EBSD detector. EBSD data was analyzed with TSL OIM software to obtain inverse pole figures (IPF), IPF maps and the grain size distribution. The grain tolerance angle for the recognition of neighbouring grains was set to 5°.

3. Results and discussion

Fig. 1 shows the polarization curves and current transients for all five substrates, for the first (a), and second (b) anodization. The curves were intentionally kept in the same scales in order to see differences between both anodizations. For the first anodization, in all cases, the curves showed the typical behaviour for the anodization of Ti in ethylene glycol, as reported earlier [14]. Briefly, within polarization curves the current increased with increasing potential until a maximum was reached, corresponding to the formation of a compact oxide layer on the Ti surface. This was typically the case shortly before or when the final potential of 60 V

was reached. Afterwards a fast current decay was observed within the current transients. When a minimum in current density was reached (typically after a few minutes from the beginning), small pores began to form randomly in the oxide layer. Due to a larger active area the current increased again until a maximum number of pores was developed, corresponding to a second maximum in current density. Subsequently, the pores grew in length and the current density decreased slowly towards a steady-state value.

Small differences in the behaviour of the substrates, i.e. in the time needed to reach the first maximum, can be explained by differences in the roughness of the surfaces in line with the reported literature [30]. These differences appear from the rolling of the Ti substrates, imprinting rolling lines into the surface.

As can be seen in Fig. 1b, all five substrates showed a similar behaviour within the second anodization. The differences in the current density between the five substrates became comparably smaller. This is likely due to the fact that the initial surface before the anodization was similar, i.e. a smooth surface with the imprints (dimples) of the first nanotube layer [26]. In addition, the current densities at the end of the second anodization (approx. 2-3 mA/cm^2 after 6 hours) were comparable to the current densities during the first anodization (after 6 hours).

In order to quantify the current densities recorded during the electrochemical anodization, a comparison of the passed charge through the nanotube layers was performed. Charge densities were considered from the beginning of the anodization till a total time of 6 hours and very comparable results were gained. For example, for the GoFe99.99% substrate charges of 58.7 C/cm^2 and 59.9 C/cm^2 were obtained for the first and second anodization, respectively. As a matter of fact, the faradaic efficiency of the tube growth is nearly the same, regardless the number anodization runs and regardless the substrate morphology for the tube growth.

Fig. 2 depicts the top views (left column) and a detailed view on the cross sections (right column) of the nanotube layers after the second anodization on the different substrates. The top views of the nanotubes revealed locally ordered nanotubes on all substrates. However, variations in the diameter of the nanotubes were observed, and the nanotube layers showed some cracks at the uppermost part of the layer.

Remarkably, as observed from the detailed inspection of the tube cross sections, in most cases the nanotubes had ripples while for the GoFe99.99% substrate, very smooth tubes were observed. For the CP substrate some intermediate state was observed - some of the nanotubes were smooth while some had ripples. The reasons for this remain unclear. However, it might be due to differences in the Ti microstructure, in particular in the different grain sizes and orientations. Investigations in this regard still have to be carried out.

Fig. 3a shows a summary of the inner nanotube diameters for all investigated nanotube layers, shown in Fig. 2. Obviously, the Ti substrate type has an influence on the inner tube diameter. This might be connected to the initial roughness of the substrate [30]. In the case of a rough, non-polished original substrate, the anodization and removal of the nanotube layer smoothed the surface of the substrate. In comparison to the first anodization, the tube formation during the second anodization was directed by the dimples on the surface of the substrate, presumably facilitating the beginning of the nanotube development.

Furthermore, it is evident that a lower tube diameter was obtained during the second anodization. This phenomenon presumably originates from the different morphology of the substrate after the first anodization, when compared to the initial substrates. That means, the starting substrates for the second anodization have smoother surfaces with dimples that act as pre-defined initiation sites. As a result, there is a shift of average inner tube diameters to lower values within the second anodization. Since for all anodizations electrolytes of exactly the same age were employed (the influence of the electrolyte aging was reported recently

[37]) a change of conductivity in the electrolyte cannot be the reason for the changes in the nanotube diameters.

However, thorough investigations of the tube dimensions showed not just large differences in the inner tube diameter of the nanotubes, but in the nanotube length as well, as plotted in Fig. 3b. The nanotube lengths after the first anodization varied between ~50 µm on the substrates SiAl and GoFe99.6+% and ~65 µm on the substrate AM. After the second anodization the longest nanotubes were found on the CP substrate with an average length of ~50 µm while again GoFe99.6+% revealed the shortest tubes with ~32 µm. Considering the anodization times of 14 hours for the first anodization and 6 hours for the second anodization it is not surprizing that in average longer tubes were obtained within the first anodization. This is simply due to longer anodization time used. An interesting conclusion can be made from Fig. 3 about the trends achieved for different substrates in terms of both the tube diameter and length. The shortest tubes and the smallest diameter tubes were for both anodizations obtained for the GoFe 99.6% substrates. In contrary, the longest tubes and the largest diameter nanotubes were obtained for the CP substrates, except that AM substrate revealed longest tubes during the first anodization (which is not an experimental error). For all other substrates, the trends were identical between the first and second anodization. This interesting violation for the AM substrates might be caused by significantly different starting substrate, compared to other ones.

In order to further elucidate differences between the substrates and the resulting nanotube layers, the bottom part of the nanotube layers were thoroughly investigated by SEM and AFM after the second anodization. The left column in Fig. 4 shows SEM bottom views of the nanotube layers after the second anodization. It is obvious, that the nanotube bottoms were locally well ordered (as also apparent from their tops, shown in Fig. 2), but still exhibited diameter variations on different locations. In addition, some minor variations in the flatness

of the tube layer can be seen. These variations presumably stem from the roughness of the Ti substrates. As evident, the Ti substrate GoFe99.99% exhibited comparably the smoothest surface of all five substrates, followed by the SiAl substrate. These results were confirmed by AFM measurements of the substrates, as shown in the right column of Fig. 4. The AFM measurements were taken from the substrate surfaces following quantitative removal of the nanotube layers. The Z scale (on the right side of each image) provides the roughness variation of the dimpled area on the Ti substrate, after removal of nanotubes grown during the second anodization.

In addition, profilometric measurements were carried out to evaluate i) the initial roughness of the Ti substrates before the first anodization and ii) the depth differences between the surface after the second anodization and the initial non-anodized Ti surface. The results are summarized in Table 1. Evidently, in the case of CP the anodization led to the deepest crater while in the case of GoFe99.6+% the shallowest crater was received. This is in accordance with the measured nanotube length in Fig. 3b: longer tubes were accompanied by a deeper crater in the Ti. Generally, the measured values of nanotube length are higher than the depth measured by the profilometer. This interesting observation can be explained by the fact that the nanotubes are growing to the depth as well as to the height, which is in line with previous literature [38].

Significant differences were also observed in terms of the initial roughness of the foil. By comparing the initial profilometric roughness of Ti with the AFM roughness of the dimpled Ti substrates after the second anodization, a match between both types of roughness was revealed, except for AM substrates. In other words, the rougher the substrates were before anodization, the rougher was the anodized area on the substrates after the second anodization. However, the AM substrate showed the highest initial roughness but the second lowest roughness after the anodizations. This can be explained by observations from the optical

microscope that revealed that AM substrates have on their surfaces some Ti stumps originating from the materials processing, except rolling lines which are present on all substrates. The stump regions occupy approximately 2-5% of the whole substrate area. The substrates are otherwise comparably rough as the other substrates. However, the presence of stumps (or, say, increased roughness of this particular substrate) could be the reason, why the tubes grown during the first anodization on this substrate were the longest from all substrates, as evident from Fig. 3b However, the stumps dissolved within the first anodization. As a result, they did not influence the roughness of this Ti substrate and corresponding tube dimensions after the second anodization. Nevertheless, the general trend that upon repetitive anodizations all substrates become smoother is very obvious from the presented results. These observations might have implications for example on the preparation of highly uniform and robust TiO_2 nanotubular membranes.

To gain more insight about the differences in the nanotube length among the different Ti substrates, the chemical composition of the substrates was analysed using GD-OES. Table 2 summarizes the Ti content and the 3 main impurities. In all cases, except for GoFe99.99%, Fe was the main impurity. Interestingly, the CP substrate had a comparably high content of V that was not one of the main impurities in other substrates. From the electrochemical point of view, vanadium oxides are much less stable in water containing electrolytes compared to TiO_2 [39]. In our water-containing electrolytes, and in the contrary to Ti, V does hardly form any oxide during anodization. In fact, it mainly dissolves in the electrolyte. Another proof of an accelerated field-aided dissolution of the CP substrate is the highest current density recorded for it (see Fig. 1). The field-aided dissolution of the growing oxides is more pronounced compared to other ones. This is a possible explanation for the deepest crater and longest tubes measured in case of CP. On the other hand, GoFe99.99% was the substrate with the highest purity of Ti. As a consequence, the substrate contained a lower quantity of

impurities which form oxides faster during anodization than Ti or only dissolve. Therefore, the nanotubes received at this substrate were the shortest. These results suggest that the purity of the Ti substrates plays an important role in terms of the consumption of the substrates and the aspect ratio of the TiO_2 nanotube layer.

Finally, the microstructure of all Ti substrates was analysed by EBSD. Fig. 5a shows the IPF map of the substrate with the smallest grains, GoFe99.99%, and Fig. 5b the IPF map of the substrate with the largest grains, CP. Fig. 5c and 5d shows grain size distributions of corresponding substrates. The difference in the grain sizes between these two substrates is approximately 20-fold. Grain sizes in all other substrates are within this range. Different grain sizes stem from different thermomechanical treatments of the Ti substrates by producers. However, the microstructure is also connected to the impurities in the Ti substrates (compare with Table 2), since the impurities significantly influence, for example, recrystallization processes and grain growth during thermomechanical treatment of the substrates [40]. GoFe99.99% is the purest substrate with just very few impurities, but possesses the smallest grain size. This is rather surprising as very pure materials usually tend to grain growth more easily than counterparts with higher impurity content. Fig. 5e and 5f shows preferential orientation of crystallites of corresponding substrates via inverse pole figures. Strong texture clearly indicates wrought (rolled) nature of the substrates. Similar texture is revealed on essentially all substrates, as the majority of the grains are close to the (0001) orientation.

One would expect that the grain size must have an influence on the ordering of the tubes. Indeed, as can see in Fig.4, there are different sizes of ordered patterns on the substrates. On GoFe99.99% substrate, there is a higher number of small locally ordered patterns, whereas on the CP substrate, there is a lower number of locally ordered large patterns. From the practical point of view, an effort to make extremely ordered nanotube layers over large areas (i.e. to

achieve large patterns of hexagonally arranged nanotubes, similar to porous alumina [24,25]), may require specific microstructures of the substrates, such us single-crystalline, nano-crystalline or highly deformed yet un-recrystallized microstructures. However, due to complex microstructural character of polycrystalline solids it is not feasible to make general conclusions and further work is necessary to rationalize an exact influence of the microstructure.

Conclusions

In summary, the influence of different Ti substrates on the nanotube growth and dimensions has been demonstrated in this work. It is obvious that the selection of the Ti substrate, even though identical conditions are used for the anodization, has a great impact on the nanotube features, namely on their diameter, length and ordering. For all substrates lower average tube diameters were revealed after the second anodization. The longest nanotubes were received for the AM substrate after the first anodization and for the CP substrate after the second anodization. The utilization of the GoFe99.99% substrate led to the highest level of ordering from all substrates, owing to the smoothest surface. Analyses of the Ti composition identified major impurities that might be the reason for different aspect ratios of the obtained nanotube layers. Furthermore, the EBSD analysess unambiguously indicate that the microstructure plays an important role for the ordering of the nanotube layers, though further work is needed to explain an exact influence of all microstructural features on the tube growth. In conclusion, the results show interesting differences between the substrates which should be considered for future anodization efforts.

Acknowledgements

ERC and the Czech Science Foundation are acknowledged for financial support of this work through projects 638857 and 14-20744S, respectively. The authors would also like to thank the project CZ.1.05/4.1.00/11.0251 „Center of Materials and Nanotechnologies“ cofinanced by the European Fund of the Regional Development, and the state budget of the Czech Republic. Ales Jäger and Karel Tesař acknowledge the financial support provided by the Czech Science Foundation (GBP108/12/G043). Mr. Jan Prikryl is acknowledged for the technical assistance with the substrates.

References

[1] M. Assefpour-Dezfuly, C. Vlachos, E. H. Andrews, Oxide morphology and adhesive bonding on titanium surfaces, J. Mater. Sci. 19 (1984) 3626.

[2] V. Zwilling, M. Aucouturier, E. Darque-Ceretti, Anodic oxidation of titanium and TA6V alloy in chromic media. An electrochemical approach, Electrochim. Acta 45 (1999) 921.

[3] J. M. Macak, H. Tsuchiya, A. Ghicov, P. Schmuki, Dye-sensitized anodic TiO_2 nanotubes, Electrochem. Commun. 7 (2005) 1133.

[4] K. Zhu, N. R. Neale, A. Miedaner, A. J. Frank, Enhanced charge-collection efficiencies and light scattering in dye-sensitized solar cells using oriented TiO_2 nanotubes arrays, Nano Lett. 7 (2007) 69.

[5] D.-J. Yang, H. Park, S.-J. Cho, H.-G. Kim, W.-Y. Choi, TiO_2-nanotube-based dye-sensitized solar cells fabricated by an efficient anodic oxidation for high surface area, J. Phys. Chem. Solids 69 (2008) 1272.

[6] P. Roy, D. Kim, K. Lee, E. Spiecker, P. Schmuki, TiO_2 nanotubes and their application in dye-sensitized solar cells, Nanoscale 2 (2010) 45.

[7] J. Liang, G. Zhang, Y. Yang, J. Zhang, Highly ordered hierarchical TiO_2 nanotube arrays for flexible fiber-type dye-sensitized solar cells, J. Mater. Chem. A 2 (2014) 19841.

[8] O. K. Varghese, D. Gong, M. Paulose, K. G. Ong, C. A. Grimes, Hydrogen sensing using titania nanotubes, Sens. Actuators, B 93 (2003) 338.

[9] D.-W. Wang, H.-T. Fang, G. Q. Lu, Z. H. Jiang, H.-M. Cheng, Amorphous TiO_2 nanotube arrays for low-temperature oxygen sensors, Nanotechnology 19 (2008) 405504.

[10] J. Lee, D. H. Kim, S.-H. Hong, J. Y. Jho, A hydrogen gas sensor employing vertically aligned TiO_2 nanotube arrays prepared by template-assisted method, Sens. Actuators, B 160 (2011) 1494.

[11] M. Kalbacova, J.M. Macak, F. Schmidt-Stein, C.T. Mierke, P. Schmuki, TiO_2 nanotubes: photocatalyst for cancer cell killing, Phys. Stat. Sol. (RRL) 2 (2008) 194.

[12] J. M. Macak, M. Zlamal, J. Krysa, P. Schmuki, Self-organized TiO_2 nanotube layers as highly efficient photocatalysts, Small 3 (2007) 300.

[13] Z. Liu, X. Zhang, S. Nishimoto, T. Murakami, A. Fujishima, Efficient photocatalytic degradation of gaseous acetaldehyde by highly ordered TiO_2 nanotube arrays, Environ. Sci. Technol. 42 (2008) 8547.

[14] J. M. Macak, H. Tsuchiya, A. Ghicov, K. Yasuda, R. Hahn, S. Bauer, P. Schmuki, TiO_2 nanotubes: Self-organized electrochemical formation, properties and applications, Curr. Opin. Solid State Mater. Sci. 11 (2007) 3.

[15] D. Kowalski, D. Kim, P. Schmuki, TiO_2 nanotubes, nanochannels and mesosponge: Self-organized formation and applications, Nanotoday 8 (2013) 235.

[16] K. Lee, A. Mazare, P. Schmuki, One-dimensional titanium dioxide nanomaterials: nanotubes, Chem. Rev. 114 (2014) 9385.

[17] J. M. Macak, H. Hildebrand, U. Marten-Jahns, P. Schmuki, Mechanistic aspects and growth of large diameter self-organized TiO_2 nanotubes, J. Electroanal. Chem. 621 (2008) 254.

[18] K. Kant, D. Losic, Self-ordering electrochemical synthesis of TiO_2 nanotube arrays: controlling the nanotube geometry and the growth rate, Int. J. Nanosci. 10 (2011) 55.

[19] L. Yin, S. Ji, G. Liu, G. Xu, C. Ye, Understanding the growth behavior of titania nanotubes, Electrochem. Commun. 13 (2011) 454.

[20] R. Beranek, H. Hildebrand, P. Schmuki, Self-organized porous titanium oxide prepared in H_2SO_4/ HF electrolytes, Electrochem. Solid-State Lett. 6 (2003) B12.

[21] J. M. Macak, H. Tsuchiya, L. Taveira, S. Aldabergerova, P. Schmuki, Smooth anodic TiO_2 nanotubes, Angew. Chem. Int. Ed. 44 (2005) 7463.

[22] J. M. Macak, P. Schmuki, Anodic growth of self-organized anodic TiO_2 nanotubes in viscous electrolytes, Electrochim. Acta 52 (2006) 1258.

[23] S. P. Albu, A. Ghicov, J. M. Macak, P. Schmuki, 250 μm long anodic TiO_2 nanotubes with hexagonal self-ordering, Phys. Stat. Sol. (RRL) 1 (2007) R65.

[24] H. Masuda, K. Fukuda, Ordered metal nanohole arrays made by a two-step replication of honeycomb structures of anodic alumina, Science, 268 (1995)1466.

[25] H. Masuda, H. Yamada, M. Satoh, H. Asoh, M. Nakao, and T. Tamamura, Highly ordered nanochannel-array architecture in anodic alumina, Appl. Phys. Lett., 71(1997) 2770.

[26] J. M. Macak, S. Albu, P. Schmuki, Towards ideal hexagonal self-ordering of TiO_2 nanotubes, Phys. Stat. Sol. (RRL) 1 (2007) 181.

[27] G. Zhang, H. Huang, Y. Zhang, H. L. W. Chan, L. Zhou, Highly ordered nanoporous TiO2 and its photocatalytic properties. Electrochem. Commun. 9 (2007) 2854.

[28] Wang, B. Yu, C. Wang, F. Zhou, W. Liu, A novel protocol toward perfect alignment of anodized TiO_2 nanotubes, Adv. Mater. 21 (2009) 1964.

[29] H.M. A. Javed, W. Que, X. Yin, Y. Xing, X. Liu, A. Asghar, J. Shao, L.B. Kong, Ordered crystalline TiO_2 nanohexagon arrays for improving conversion efficiency of dye-sensitized solar cells, J. Alloys Compd. 646 (2015) 106.

[30] K. Lu, Z. Tian, J. A. Geldmeier, Polishing effect on anodic titania nanotube formation, Electrochim. Acta 56 (2011) 6014.

[31] C.-C. Chen, J.-H. Chen, C.-G. Chao, W. C. Say, Electrochemical characteristics of surface of titanium formed by electrolytic polishing and anodizing, J. Mater. Sci. 40 (2005) 4053.

[32] T. Kondo, S. Nagao, T. Yanagishita, N.T. Nguyen, K.Lee, P. Schmuki, H. Masuda, Ideally ordered porous TiO_2 prepared by anodization of pretexturedTi by nonoimprinting process, Electrochem. Commun. 50 (2015) 73.

[33] J.M. Macak, B.G. Gong, M. Hueppe, P. Schmuki, Filling of TiO_2 nanotubes by self-doping and electrodeposition, Adv. Mater. 19 (2007) 3027.

[34] P. Knotek, E. Chanova, F. Rypacek, AFM imaging and analysis of local mechanical properties for detection of surface pattern of functional groups, Mater. Sci. Eng., C, 33 (2013) 1963.

[35] P. Knotek, D. Arsova, E. Vateva, L. Tichy, Photo-expansion in Ge-As-S amorphous film monitored by digital holographic microscopy and atomic force microscopy, J. Optoelectron. Adv. Mater., 11 (2009) 391.

[36] T. Kratochvil, T. Cernohorsky, P. Knotek, J. Navesnik, L. Kalina, M. Pouzar, M. Zvolska, Fast determination of the surface density of titanium in ultrathin layers using LIBS spectrometry, J. Anal. At. Spectrom., 29 (2014) 1806.

[37] H. Sopha, L. Hromadko, K. Nechvilova, J.M. Macak, Effect of eectrolyte age and potential changes on the morphology of TiO_2 nanotubes, J. Electroanal. Chem., in press, doi:10.1016/j.jelechem.2015.11.002.

[38] S. Albu, P. Schmuki, Influence of anodization parameters on the expansion factor of TiO_2 nanotubes, Electrochim. Acta 19 (2013) 90.

[39] J.P. Schreckenbach, P. Strauch, Microstructure study of amorphous vanadium oxide films, Appl. Surf. Sci., 143 (1999) 6.

[40] M.J. Donachie: Titanium: A Technical Guide, 2nd ed., ASM International, 2007

Figure captions

Fig. 1: Polarization plots (left) and current transients (right) recorded for the anodization of different Ti substrates for the 1st anodization (a) and for the 2nd anodization (b). The curve for the 1st anodization shows initial 6 hours of the total time 14 hours.

Fig. 2: Top (left) and detailed cross section (right) views of the nanotube arrays after the second anodization. a) AM, b) SiAl, c) CP, d) GoFe99.6+%, e) GoFe99.99%. All scale bars show a distance of 100 nm.

Fig. 3: Evaluation of the average inner diameter (a) and length (b) for the first and second anodization of the different substrates.

Fig. 4. Left column: Bottom views of the TiO_2 nanotube layers after the second anodization. Right column: AFM topography of the Ti substrates after the second anodization step (measured on an area of the size 5x5 μm^2). Nanotube layers were quantitatively removed from the surfaces before these AFM measurements. a) AM, b) SiAl, c) CP, d) GoFe99.6+%, e) GoFe99.99%.

Fig. 5 Inverse pole figure maps for (a) GoFe99.99 and (b) CP substrates; (c-d) histograms of grain size distributions and (e-f) inverse pole figures for the same substrates, respectively.

Figures

Figure 1

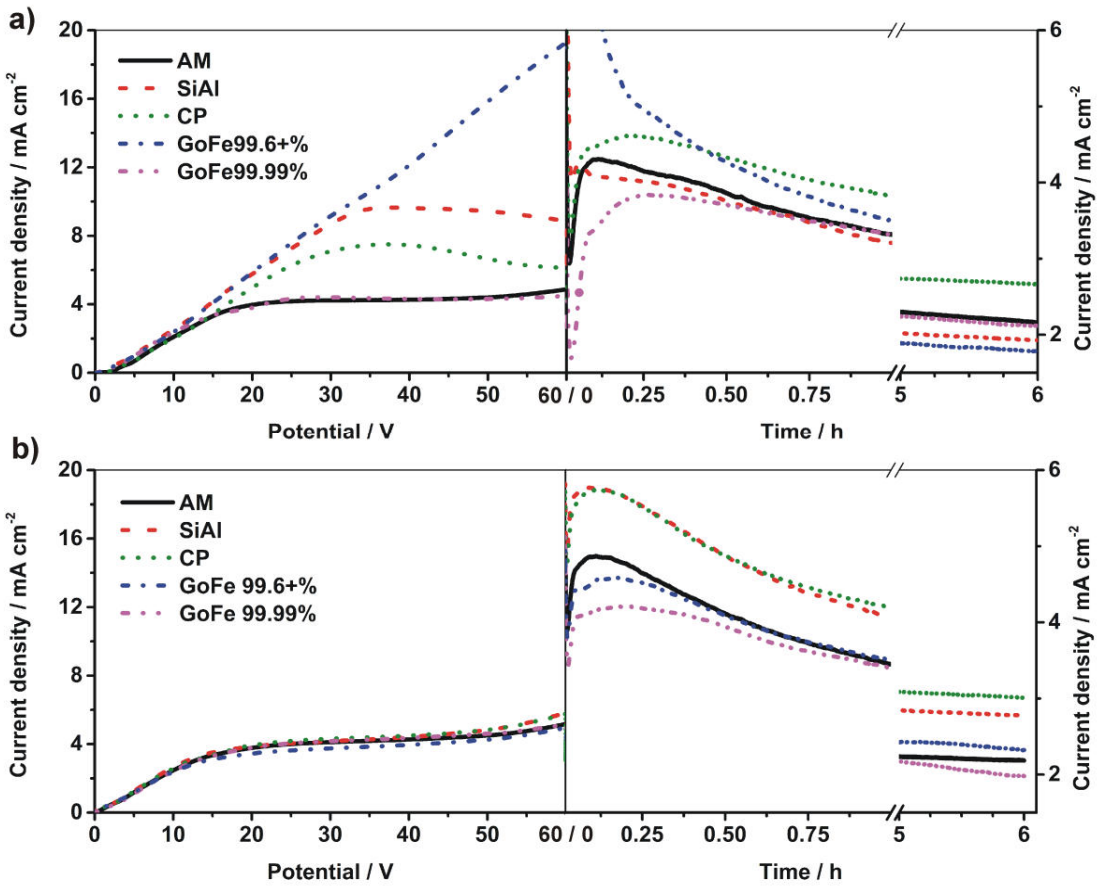

Figure 2

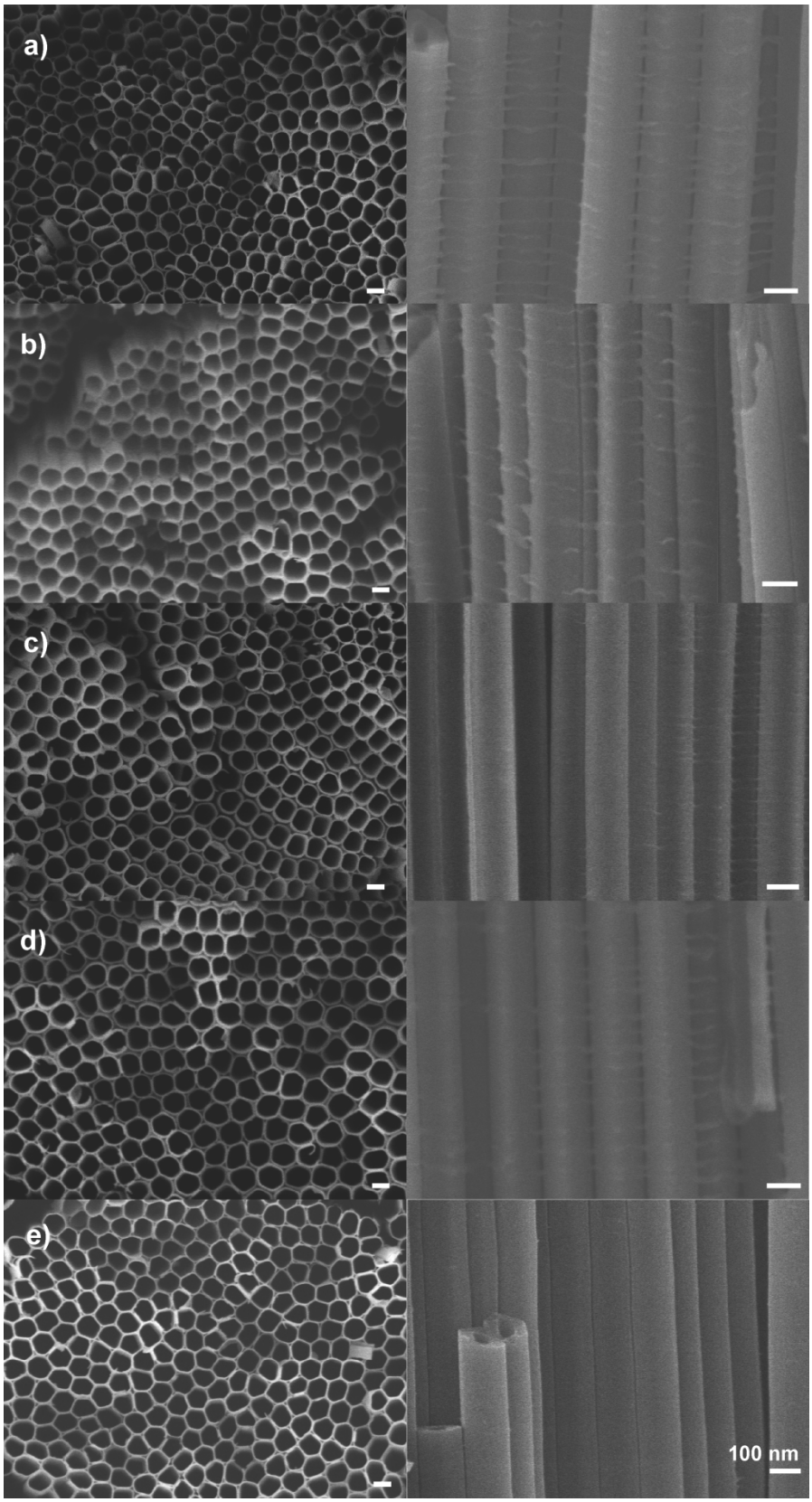

Figure 3

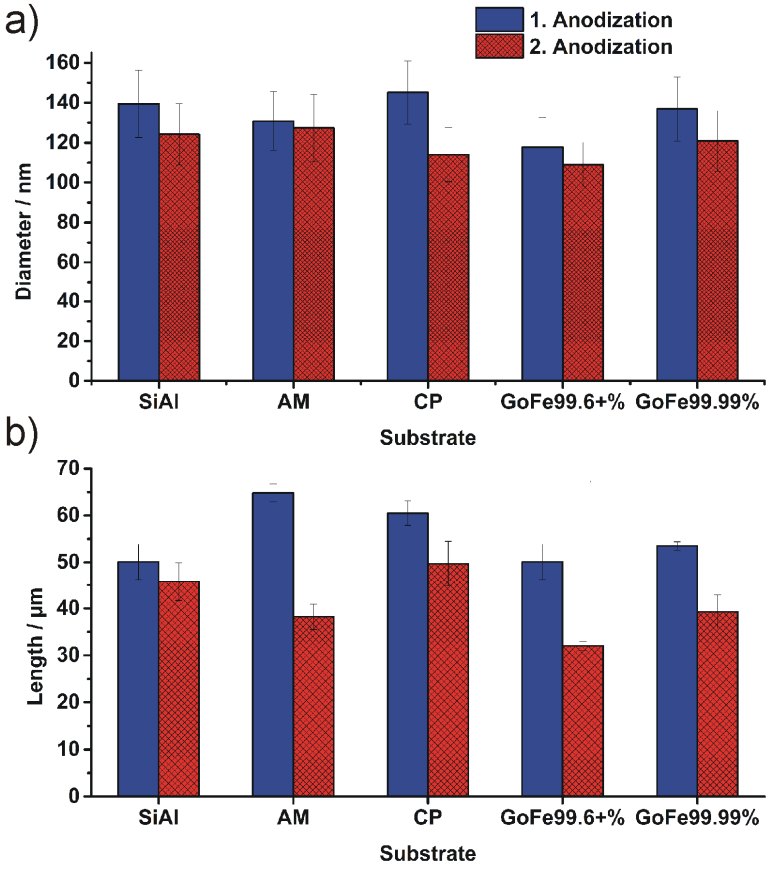
a)
1. Anodization
2. Anodization
Diameter / nm
160
140
120
100
80
60
40
20
0
SiAl
AM
CP
GoFe99.6+%
GoFe99.99%
Substrate
b)
Length / µm
70
60
50
40
30
20
10
0
SiAl
AM
CP
GoFe99.6+%
GoFe99.99%
Substrate

Figure 4

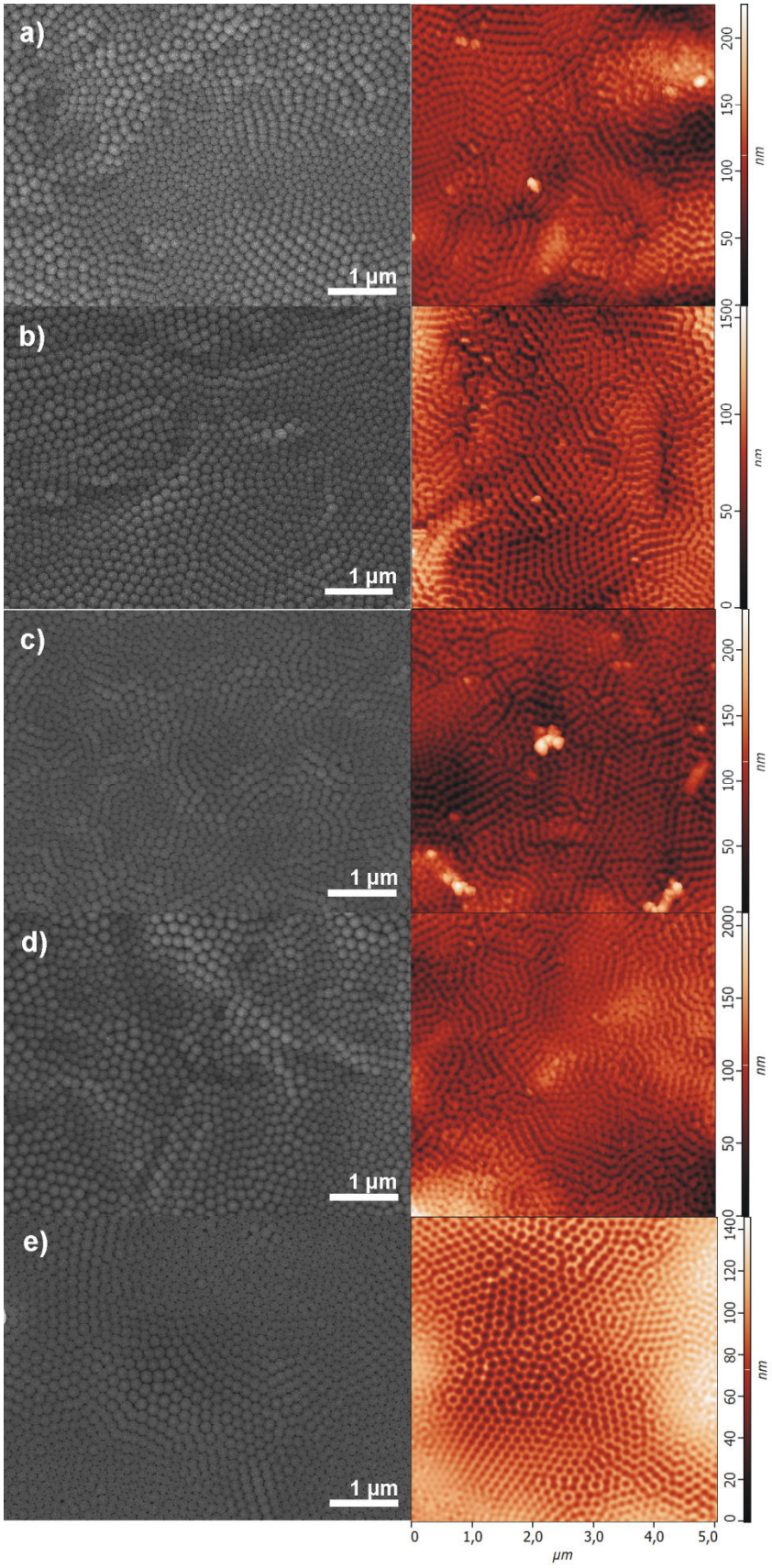

Figure 5

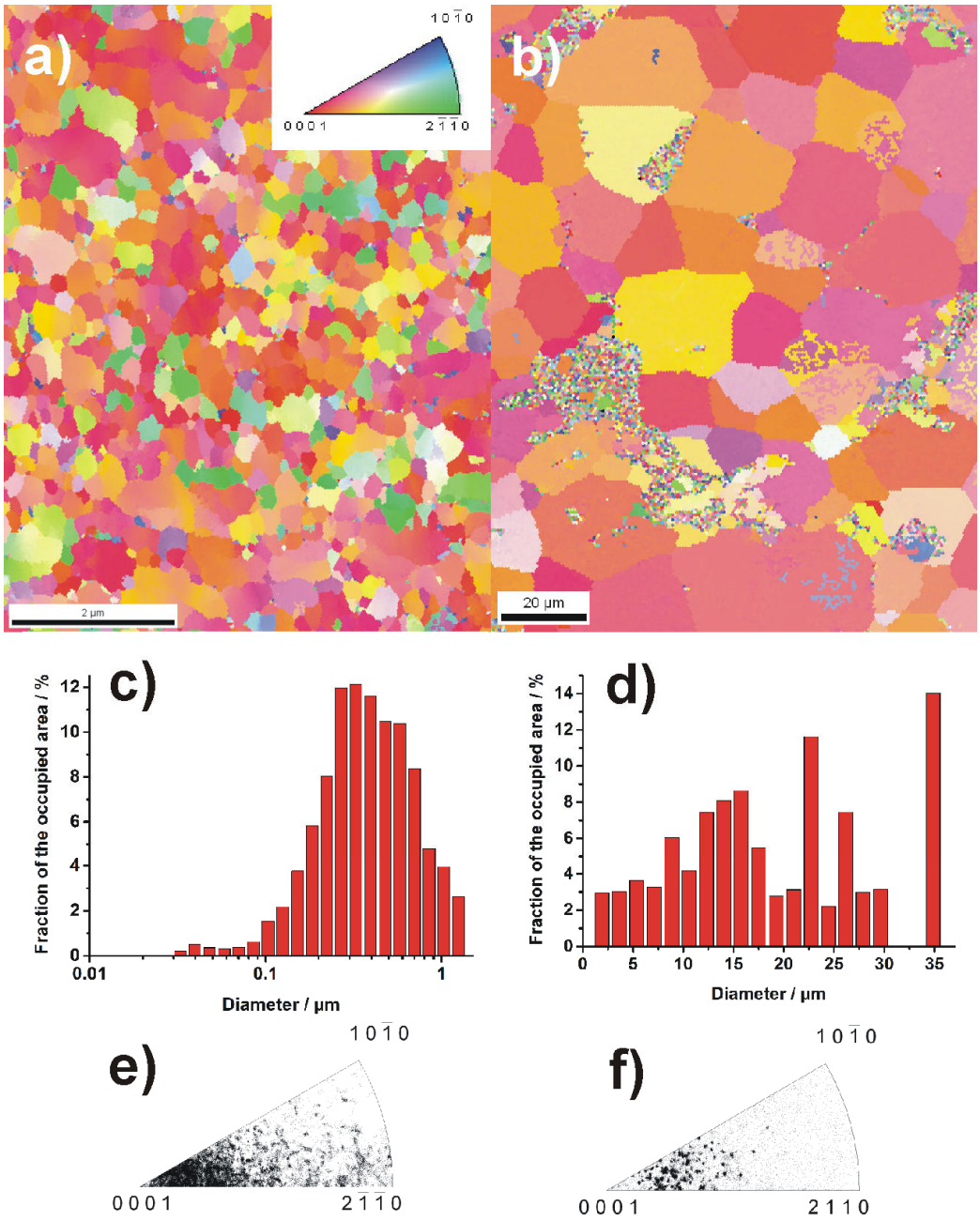
a)
b)
$10\bar{1}0$
0001
$2\bar{1}\bar{1}0$
2 µm
20 µm
c)
Fraction of the occupied area / %
Diameter / µm
d)
Fraction of the occupied area / %
Diameter / µm
e)
$10\bar{1}0$
0001
$2\bar{1}\bar{1}0$
f)
$10\bar{1}0$
0001
$2\bar{1}\bar{1}0$

Tables

Substrate	RMS of the Ti roughness before anodization (nm)	RMS of the Ti roughness after anodization (nm)	Average crater depth (µm)
AM	610 ± 80	69 ± 4	42 ± 3
SiAl	380 ± 50	82 ± 5	38 ± 3
CP	290 ± 30	77 ± 1	68 ± 7
GoFe99.6+%	130 ± 10	75 ± 0.5	35 ± 2
GoFe99.99%	25 ± 4	18 ± 1	37 ± 2

Table 1. Summary of the measured parameters of Ti and TiO_2 nanotubes: Roughness of the initial Ti substrates (acquired by DHM), roughness of the anodized Ti substrates after the second anodization (acquired by AFM) and depth difference between the anodized area after the second anodization and the non-anodized area of the Ti substrate (acquired by profilometer).

Ti sample	**Ti**	**Impurity 1**	**Impurity 2**	**Impurity 3**
AM	99.719%	Fe - 0.180%	Al - 0.036%	W - 0.011%
SiAl	99.874%	Fe - 0.036%	Cr - 0.01%	Al - 0.013%
CP	99.729%	Fe - 0.081%	V - 0.051%	Sn - 0.039%
GoFe99.6+%	99.764%	Fe - 0.109%	Al - 0.023%	Cu - 0.020%
GoFe99.99%	99.956%	Al - 0.012%	Si - 0.006%	Cu - 0.004%

Table 2. Ti content and the three main impurities of the Ti substrates measured by GD-OES, given in weight %.